# SANDIA REPORT

SAND2005-0498
Unlimited Release
Printed May 2005

# Control of a High Beta Maneuvering Reentry Vehicle Using Dynamic Inversion

A. C. Watts

Prepared by
Sandia National Laboratories
Albuquerque, New Mexico 87185 and Livermore, California 94550

Sandia is a multiprogram laboratory operated by Sandia Corporation,
a Lockheed Martin Company, for the United States Department of Energy's
National Nuclear Security Administration under Contract DE-AC04-94AL85000.



Sandia National Laboratories

Issued by Sandia National Laboratories, operated for the United States Department of Energy by Sandia Corporation.



Available to DOE and DOE contractors from
U.S. Department of Energy
Office of Scientific and Technical Information
P.O. Box 62
Oak Ridge, TN 37831

Telephone: (865)576-8401
Facsimile: (865)576-5728
E-Mail: reports@adonis.osti.gov
Online ordering: http://www.osti.gov/bridge

Available to the public from
U.S. Department of Commerce
National Technical Information Service
5285 Port Royal Rd
Springfield, VA 22161

Telephone: (800)553-6847
Facsimile: (703)605-6900
E-Mail: orders@ntis.fedworld.gov
Online order: http://www.ntis.gov/help/ordermethods.asp?loc=7-4-0#online

SAND2005-0498
Unlimited Release
Printed May 2005

# Control of a High Beta Maneuvering Reentry Vehicle Using Dynamic Inversion

A. C. Watts
Aerospace Systems Development Center
Sandia National Laboratories
P. O. Box 5800
Albuquerque, NM 87185-1174

Abstract

The design of flight control systems for high performance maneuvering reentry vehicles presents a significant challenge to the control systems designer. These vehicles typically have a much higher ballistic coefficient than crewed vehicles like as the Space Shuttle or proposed crew return vehicles such as the X-38. Moreover, the missions of high performance vehicles usually require a steeper reentry flight path angle, followed by a pull-out into level flight. These vehicles then must transit the entire atmosphere and robustly perform the maneuvers required for the mission. The vehicles must also be flown with small static margins in order to perform the required maneuvers, which can result in highly nonlinear aerodynamic characteristics that frequently transition from being aerodynamically stable to unstable as angle of attack increases. The control system design technique of dynamic inversion has been applied successfully to both high performance aircraft and low beta reentry vehicles. The objective of this study was to explore the application of this technique to high performance maneuvering reentry vehicles, including the basic derivation of the dynamic inversion technique, followed by the extension of that technique to the use of tabular trim aerodynamic models in the controller. The dynamic inversion equations are developed for high performance vehicles and augmented to allow the selection of a desired response for the control system. A six degree of freedom simulation is used to evaluate the performance of the dynamic inversion approach, and results for both nominal and off nominal aerodynamic characteristics are presented.

# Acknowledgements

The aerodynamics models used extensively in the work described in this report were developed and provided by Ron Tucker. The six degree of freedom simulation implemented using Matlab and Simulink utilized the structure and algorithms from simulations originally developed by Ron. Ron also provided derivations and notes concerning the formulation of the models and numerous other suggestions and comments. Ron's assistance and contributions to this work are gratefully acknowledged.

Ed Caicedo and Dave Outka proofread this report and corrected the author's errors in logic and mathematics. Ed provided significant assistance in insuring that the simulation used to generate the results shown in this report were consistent with the derivations presented here.

This work was funded through the Prompt Global Response Laboratory Directed Research and Development project at Sandia National Laboratories. The support of J. Mike Macha, the Project Manager in funding this work, is also gratefully acknowledged.

# Contents



# Figures

## Tables

# 1 Introduction

High performance maneuvering reentry vehicles present a significant challenge to the control system designer. As is the case with most reentry vehicles, they enter the atmosphere at high speeds and pass through a number of flight regimes prior to the end of a mission. If high maneuverability is required, the vehicle must be controlled at relatively large angles of attack where the aerodynamic characteristics are highly nonlinear. In order to achieve high angles of attack, the aerodynamic stability margin of the vehicle may necessarily be small, and the vehicle may well be aerodynamically unstable in some parts of its flight envelope. There may also be significant coupling between axes of the vehicle, particularly when flying at high angle of attack. These issues, as well as others, can make the design of the guidance and flight control system very difficult. Use of classical control system design techniques using separate linearized models for each of the three vehicle axes is difficult and relies extensively on the skill and experience of the control designer in order to yield a viable control system design.

The purpose of this report is to explore the application of a relatively new control system design approach to control systems for high performance maneuvering reentry vehicles. Such vehicles typically have high ballistic coefficients, relatively steep reentry trajectories and, typically, must pull out into level flight in order to perform a required mission. The characteristics of such vehicles are generally significantly different then crewed reentry vehicles such as the Space Shuttle or various proposed crew return vehicles.

This study will explore the application of a control system design approach known as Dynamic Inversion or Feedback Linearization to high performance maneuvering reentry vehicles. For the purposes of this study, the design approach will be applied to a proposed vehicle with a relatively sharp axi-symmetric conical body and four strakes in a cruciform arrangement. The proposed vehicle is controlled by four movable elevons located at the end of each strake. The shape of the candidate vehicle is shown in Figure 1-1.

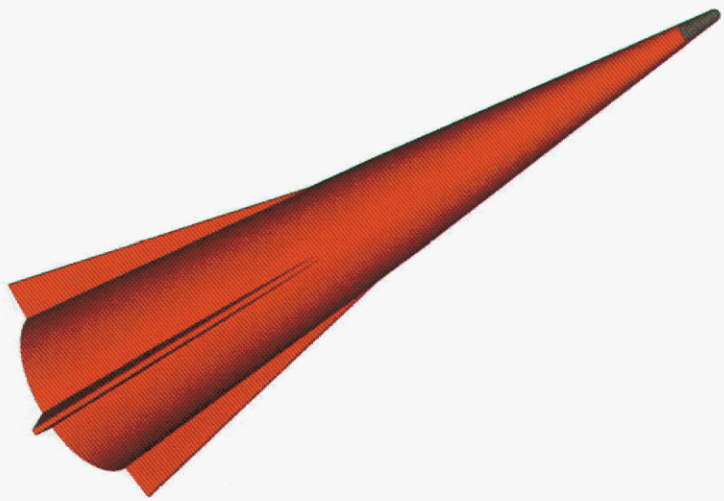

**Figure 1-1. Illustration showing the configuration of the maneuvering reentry vehicle used in this study.**

This candidate configuration was chosen partly because of its similarity to a vehicle flight tested in the mid 1980's, which was known to present a formidable challenge in the flight control system design. Extensive wind tunnel data are available for that vehicle, as well as the control system design used in those flight tests. The aerodynamic model for the vehicle used in this study was developed using computational fluid dynamics methods and extrapolation of the aerodynamic data base for the vehicle flight tested earlier.

The application of Dynamic Inversion requires a model of the system or plant to be controlled and uses that model to synthesize control inputs, which cancel the dynamics of the plant, and substitute a set of desired dynamics for the controlled system. The robustness of a design using such an approach with respect to errors in the model used is clearly a significant concern.

The methodology used in this study included development of a guidance and control system design using Dynamic Inversion for the candidate vehicle described above. A six degree of freedom simulation was developed for evaluation of the performance of that design on a typical reentry trajectory. The performance and robustness of the design was then qualitatively compared to the classical design developed for the vehicle flight tested earlier.

## 2 Dynamic Inversion

The dynamic inversion approach can be applied to an nth-order nonlinear system that can be described by a set of differential equations given by

$$\dot{\mathbf{x}}(t) = \mathbf{f}(\mathbf{x}) + \mathbf{g}(\mathbf{x})\mathbf{u}(t) \tag{2-1}$$

where $\mathbf{x}(t)$ is the state vector, $\mathbf{u}(t)$ is the control input and $\mathbf{f}(\mathbf{x})$ and $\mathbf{g}(\mathbf{x})$ are smooth functions of the system state. A system that can be represented in this form, where the control input can be separated as shown, is said to be affine in the control input. In the basic form of dynamic inversion, the control input is taken to be

$$\mathbf{u} = \mathbf{g}^{-1}(\mathbf{x})\left(\left[\dot{\mathbf{x}}\right]_{des} - \mathbf{f}(\mathbf{x})\right) \tag{2-2}$$

where $\left[\dot{\mathbf{x}}\right]_{des}$ is the desired value of the time derivative of the state vector and it is assumed that the control matrix $\mathbf{g}(\mathbf{x})$ is invertible. With suitable restrictions on $\mathbf{f}(\mathbf{x})$ and $\mathbf{g}(\mathbf{x})$, the system described by (2-1) reduces to

$$\dot{\mathbf{x}} = \left[\dot{\mathbf{x}}\right]_{des} \tag{2-3}$$

which is a system of linear first order uncoupled differential equations. A much more rigorous derivation of the dynamic inversion approach, including the various conditions of the properties of the system, can be found in Getz[1].

In general, a tabular aerodynamic model of a vehicle with control surfaces would be a function of Mach number, angle of attack and sideslip (or, alternatively, total angle of attack and aerodynamic roll angle) and the position of the control surfaces. For vehicles with even a modest number of control surfaces, this results in large multidimensional tables and high order interpolation algorithms. A more compact but less general model can be based on the assumption that the vehicle operates in the vicinity of trim points. The aerodynamic model can then be expressed in terms of tabular trim values and partial derivatives of various parameters around the trim values.

The dynamic inversion approach outlined above can be reformulated to utilize a trim model of the vehicle aerodynamics. In this case it is assumed that there is trim control input $\mathbf{u}_0(\mathbf{x})$ that causes the system to be in equilibrium at some value of the state vector. This trim control input must satisfy

$$\mathbf{u}_0(t) = -\mathbf{g}^{-1}(\mathbf{x})\mathbf{f}(\mathbf{x}). \tag{2-4}$$

The vehicle control input is assumed to be the sum of the trim control value for the current flight condition and input from the flight control system. That is, the vehicle control is taken to be

$$\mathbf{u}(t) = \mathbf{v}(t) + \mathbf{u}_0(t) \tag{2-5}$$

where $\mathbf{v}(t)$ is the flight control input and $\mathbf{u}_0(t)$ is the trim control input.

Substitution of (2-4) and (2-5) into (2-1) gives

$$\dot{\mathbf{x}} = \mathbf{f}(\mathbf{x}) + \mathbf{g}(\mathbf{x})\left[\mathbf{v}(t) + \mathbf{u}_0(t)\right] \tag{2-6}$$

$$\dot{\mathbf{x}} = \mathbf{f}(\mathbf{x}) + \mathbf{g}(\mathbf{x})\left[\mathbf{v}(t) - \mathbf{g}^{-1}(\mathbf{x})\mathbf{f}(\mathbf{x})\right] \tag{2-7}$$

$$\dot{\mathbf{x}} = \mathbf{g}(\mathbf{x})\mathbf{v}(t) \tag{2-8}$$

$$\mathbf{v}(t) = \mathbf{g}^{-1}(\mathbf{x})\left[\dot{\mathbf{x}}\right]_{des}. \tag{2-9}$$

The closed loop dynamics then reduces to the same form as (2-3) above.

## 3 Desired Dynamic Response

The dynamic inversion approach results in an equivalent system of linear uncoupled differential equations driven by the desired value of the time derivative of the state vector given by $\left[\dot{\mathbf{x}}\right]_{des}$. The properties and dynamics of the resulting closed loop system can be chosen by properly selecting the structure of that input. Taking

$$\left[\dot{\mathbf{x}}\right]_{des} = \mathbf{w}(t) \tag{3-1}$$

and using the Laplace transform

$$\mathbf{W}(s) = \mathbf{K}(s)\left[\mathbf{X}_{cmd}(s) - \mathbf{X}(s)\right] \tag{3-2}$$

$$s\mathbf{X}(s) = \mathbf{K}(s)\left[\mathbf{X}_{cmd}(s) - \mathbf{X}(s)\right] \tag{3-3}$$

$$\left[s\mathbf{I} + \mathbf{K}(s)\right]\mathbf{X}(s) = \mathbf{K}(s)\mathbf{X}_{cmd}(s). \tag{3-4}$$

The transfer function of the closed loop system is then

$$\frac{\mathbf{X}(s)}{\mathbf{X}_{cmd}(s)} = \left[s\mathbf{I} + \mathbf{K}(s)\right]^{-1}\mathbf{K}(s). \tag{3-5}$$

Suppose the desired closed loop transfer function is

$$\frac{\mathbf{X}(s)}{\mathbf{X}_{cmd}(s)} = \mathbf{D}(s). \tag{3-6}$$

The transfer function of the dynamic inversion controller can then be found from

$$\mathbf{D}(s) = \left[s\mathbf{I} + \mathbf{K}(s)\right]^{-1}\mathbf{K}(s) \tag{3-7}$$

$$\mathbf{K}(s) = [s\mathbf{I} + \mathbf{K}(s)]\mathbf{D}(s) \tag{3-8}$$

$$\mathbf{K}(s) - \mathbf{K}(s)\mathbf{D}(s) = s\mathbf{D}(s) \tag{3-9}$$

$$\mathbf{K}(s)[\mathbf{I} - \mathbf{D}(s)] = s\mathbf{D}(s) \tag{3-10}$$

$$\mathbf{K}(s) = s\mathbf{D}(s)[\mathbf{I} - \mathbf{D}(s)]^{-1}. \tag{3-11}$$

The dynamic inversion flight control system is likely to be an inner part of a guidance or steering loop. The performance and stability of this system may require shaping of the response of the controlled vehicle. Two desired closed loop transfer functions will be considered, and the required form of the dynamic inversion controller derived.

## 3.1 1st Order Dynamics

Suppose that the desired response can be represented by a first order transfer function with unity gain at zero frequency with a break frequency of $\omega_0$. The desired transfer function is then

$$D(s) = \frac{\omega_0}{s + \omega_0}. \tag{3-12}$$

Equation (3-11) then gives

$$\begin{aligned} K(s) &= \left(\frac{s\omega_0}{s + \omega_0}\right)\left[1 - \left(\frac{\omega_0}{s + \omega_0}\right)\right]^{-1} \\ &= \omega_0 \end{aligned} \tag{3-13}$$

The control is then

$$u(t) = u_0(t) + g^{-1}(x)\omega_0[x_{cmd}(t) - x(t)]. \tag{3-14}$$

## 3.2 2nd Order Dynamics

If a classic second order response is desired then we can take

$$D(s) = \frac{\omega_n^2}{s^2 + 2\xi\omega_n s + \omega_n^2}. \tag{3-15}$$

Using the same procedure we can find the required controller transfer function to yield the desired dynamics. Equation (3-11) gives

$$K(s) = \frac{s\omega_n^2}{s^2 + 2\xi\omega_n s + \omega_n^2}\left[1 - \frac{\omega_n^2}{s^2 + 2\xi\omega_n s + \omega_n^2}\right]^{-1} \tag{3-16}$$

which reduces to

$$K(s) = \frac{\omega_n^2}{s + 2\xi\omega_n}. \tag{3-17}$$

The controller then becomes

$$\dot{w}(t) = -2\xi\omega_n w(t) + \omega_n^2\left[x_{cmd}(t) - x(t)\right]. \tag{3-18}$$

# 4 Application to Maneuvering Reentry Vehicles

The implementation of a dynamic inversion controller depends on the assumption that the control matrix $\mathbf{g}(x)$ is invertible. The properties of the controller will clearly depend on the properties of this matrix and its inverse. The terms which generally appear in a classical control system design frequently involve the inverse of the various terms in the control matrix and also depend on these terms being well conditioned. The derivation of the dynamic inversion approach presented above was based on a general system and assumed that complete knowledge of the state of that system is available. It should not be surprising that the successful application of the dynamic inversion approach depends on careful selection to the model of the system and the states to be controlled. Difficulties with the inversion of the control matrix $\mathbf{g}(x)$ can be addressed by careful selection of the dynamics to be inverted and by partitioning the inversion into slow and fast dynamic sections[2]. The original system can be partitioned into two sets of coupled differential equations, and the dynamic inversion approach applied to each separately. The fast or short period dynamics are taken to include the body angular rates and the moments acting on the vehicle. The slow or long period dynamics are taken to include the body attitude and velocity, which can be combined into the angle of attack and angle of sideslip. The resulting structure will be seen to be very similar to the classical inner / outer loop structure used in many or most flight control systems.

## 4.1 Short Period Inversion

The differential equations for the angular rates of the body may be written as

$$\mathbf{I}\dot{\boldsymbol{\omega}} = -\boldsymbol{\Omega}_{\mathbf{ib}}^{\mathbf{b}}\mathbf{I}\boldsymbol{\omega} + \mathbf{M}_{aero}^{b} \tag{4-1}$$

where

$$\boldsymbol{\omega} = \begin{bmatrix} p & q & r \end{bmatrix}' \tag{4-2}$$

and

$$\boldsymbol{\Omega}_{ib}^{b} = \begin{bmatrix} 0 & -r & q \\ r & 0 & -p \\ -q & p & 0 \end{bmatrix} \tag{4-3}$$

and $\mathbf{I}$ is the inertia tensor or dyadic. The aerodynamic moments are assumed to have the form

$$\mathbf{M}_a = \mathbf{m}_a(\alpha_T, \varphi_a) + \mathbf{g}_a(\alpha_T, \varphi_a)\mathbf{u}\,. \tag{4-4}$$

The model will be based on a trim elevon deflection given by

$$\mathbf{u}_0(\alpha_T, \phi_a) = -\mathbf{g}_a^{-1}(\alpha_T, \phi_a)\mathbf{m}_a(\alpha_T, \phi_a)\,. \tag{4-5}$$

The elevon commands will be taken as the sum of the trim value and a control input as developed in the dynamic inversion formulation above

$$\mathbf{u} = \mathbf{v} + \mathbf{u}_0(\alpha_T, \phi_a)\,. \tag{4-6}$$

The aerodynamic moment is then

$$\mathbf{M}_a = \mathbf{g}_a(\alpha_T, \varphi_a)\mathbf{v}\,, \tag{4-7}$$

and the differential equations for body angular rates are

$$\mathbf{I}\dot{\boldsymbol{\omega}} = \left[\mathbf{g}_a(\alpha_T, \varphi_a)\mathbf{v} - \boldsymbol{\Omega}_{ib}^{b}\mathbf{I}\boldsymbol{\omega}\right]. \tag{4-8}$$

The control input is

$$\mathbf{v} = \mathbf{g}_a^{-1}(\alpha_T, \varphi_a)\left[\mathbf{I}\left[\dot{\boldsymbol{\omega}}\right]_{des} + \boldsymbol{\Omega}_{ib}^{b}\mathbf{I}\boldsymbol{\omega}\right]. \tag{4-9}$$

For the fast inversion loop we use first order desired dynamics as shown above, which gives

$$\left[\dot{\boldsymbol{\omega}}\right]_{des} = \mathbf{K}(\boldsymbol{\omega}_{cmd} - \boldsymbol{\omega}) \tag{4-10}$$

where

$$\mathbf{K} = \begin{bmatrix} k_x & 0 & 0 \\ 0 & k_y & 0 \\ 0 & 0 & k_z \end{bmatrix}. \tag{4-11}$$

The fast loop command is then

$$\mathbf{u} = \mathbf{u}_0(\alpha_T, \phi_a) + \mathbf{g}_a^{-1}(\alpha_T, \phi_a)\left[\mathbf{I}\mathbf{K}(\boldsymbol{\omega}_{cmd} - \boldsymbol{\omega}) + \boldsymbol{\Omega}_{ib}^{b}\mathbf{I}\boldsymbol{\omega}\right]. \tag{4-12}$$

## 4.2 Long Period Inversion

The long period inversion section will control an Euler roll angle, defining the roll orientation of the body with respect to the earth, the angle of attack and the angle of sideslip. The variables to be controlled are

$$\phi = \tan^{-1}\left(\frac{C_{dy}}{C_{dz}}\right), \tag{4-13}$$

$$\alpha = \tan^{-1}\left(\frac{w}{u}\right) \tag{4-14}$$

and

$$\beta = \tan^{-1}\left(\frac{v}{u}\right). \tag{4-15}$$

The elements in the expression for Euler roll angle in (4-13) are elements of the direction cosine matrix, which is the transformation from body to navigation coordinates given by

$$\mathbf{C}_b^n = \begin{bmatrix} C_{nx} & C_{ny} & C_{nz} \\ C_{ex} & C_{ey} & C_{ez} \\ C_{dx} & C_{dy} & C_{dz} \end{bmatrix}. \tag{4-16}$$

This transformation is naturally computed by strapdown inertial navigation systems either directly or in the form of quaternions, which may be used to compute the required transformation. The elements in the expression for angle of attack and angle of sideslip are body components of velocity where

$$\mathbf{v}^b = \begin{bmatrix} u & v & w \end{bmatrix}'. \tag{4-17}$$

An inertial navigation system generally computes velocity in a navigation coordinate system, but these are readily expressed in body velocities as

$$\mathbf{v}^b = \mathbf{C}_n^b \mathbf{v}^n. \tag{4-18}$$

The time derivatives of the roll angle, angle of attack and angle of sideslip are given by

$$\dot{\alpha} = \frac{u\dot{w} - w\dot{u}}{u^2 + w^2}, \tag{4-19}$$

$$\dot{\beta} = \frac{u\dot{v} - v\dot{u}}{u^2 + v^2} \tag{4-20}$$

and

$$\dot{\phi} = \frac{C_{dz}\dot{C}_{dy} - C_{dy}\dot{C}_{dz}}{C_{dz}^2 + C_{dy}^2}. \tag{4-21}$$

The derivatives required in the roll angle expression are found from the Coriolis equation as

$$\dot{\mathbf{C}}_b^n = \mathbf{C}_b^n \boldsymbol{\Omega}_{nb}^b \tag{4-22}$$

or

$$\dot{\mathbf{C}}_b^n = \begin{bmatrix} C_{nx} & C_{ny} & C_{nz} \\ C_{ex} & C_{ey} & C_{ez} \\ C_{dx} & C_{dy} & C_{dz} \end{bmatrix} \begin{bmatrix} 0 & -r & q \\ r & 0 & -p \\ -q & p & 0 \end{bmatrix} \tag{4-23}$$

which gives

$$\dot{C}_{dy} = pC_{dz} - rC_{dx} \tag{4-24}$$

and

$$\dot{C}_{dz} = qC_{dx} - pC_{dy}. \tag{4-25}$$

The time derivatives of the body velocity terms can be found from differentiation of (4-18)

$$\dot{\mathbf{v}}^b = \mathbf{C}_n^b \dot{\mathbf{v}}^n + \dot{\mathbf{C}}_n^b \mathbf{v}^n. \tag{4-26}$$

From Newton's 2nd law with the forces acting on the system divided into aerodynamic and gravitational force components and neglecting the centripetal and Coriolis acceleration terms, the derivative of velocity in navigation coordinates is

$$\dot{\mathbf{v}}^n = \frac{1}{m}(\mathbf{f}_{aero}^n + \mathbf{f}_{gravity}^n) \tag{4-27}$$

where m is the mass of the vehicle.

$$\begin{aligned} \dot{\mathbf{v}}^n &= \frac{1}{m}(\mathbf{C}_b^n \mathbf{f}_{aero}^b + \mathbf{f}_{gravity}^n) \\ &= \frac{1}{m}\mathbf{C}_b^n \mathbf{f}_{aero}^b + \mathbf{a}_{gravity}^n \end{aligned} \tag{4-28}$$

Using the transformation properties of ortho-normal matrices, the time derivative of the velocity in body coordinates is then

$$\dot{\mathbf{v}}^b = \mathbf{C}_n^b \dot{\mathbf{v}}^n + (\dot{\mathbf{C}}_b^n)' \mathbf{v}^n \tag{4-29}$$

or

$$\dot{\mathbf{v}}^b = \mathbf{C}_n^b \dot{\mathbf{v}}^n + (\mathbf{C}_b^n \boldsymbol{\Omega}_{nb}^b)' \mathbf{v}^n . \tag{4-30}$$

This can be rewritten by substitution of (4-28) and by expressing the aerodynamic forces in body coordinates and the acceleration of gravity in navigation coordinates as

$$\begin{aligned} \dot{\mathbf{v}}^b &= \mathbf{C}_n^b \dot{\mathbf{v}}^n - \boldsymbol{\Omega}_{nb}^b \mathbf{C}_n^b \mathbf{v}^n \\ &= \frac{1}{m} \mathbf{C}_n^b \mathbf{C}_b^n \mathbf{f}_{aero}^b + \mathbf{a}_{gravity}^b - \Omega_{nb}^b \mathbf{v}^b \\ &= \frac{1}{m} \mathbf{f}_{aero}^b + \mathbf{C}_n^b \mathbf{a}_{gravity}^n - \Omega_{nb}^b \mathbf{v}^b \end{aligned} \tag{4-31}$$

which expands to

$$\dot{\mathbf{v}}^b = \frac{1}{m} \mathbf{f}_{aero}^b + \mathbf{C}_n^b \mathbf{a}_{gravity}^n + \begin{bmatrix} 0 & r & -q \\ -r & 0 & p \\ q & -p & 0 \end{bmatrix} \mathbf{v}^b \tag{4-32}$$

$$\begin{bmatrix} \dot{u} \\ \dot{v} \\ \dot{w} \end{bmatrix} = \begin{bmatrix} rv - qw \\ pw - ru \\ qu - pv \end{bmatrix} + \left( \frac{1}{m} \right) \begin{bmatrix} f_x \\ f_y \\ f_z \end{bmatrix} + \begin{bmatrix} C_{dx} \\ C_{dy} \\ C_{dz} \end{bmatrix} g \tag{4-33}$$

where we have neglected all but the vertical component of gravity.

The time derivatives of the roll angle, angle of attack and angle of sideslip can then be written as

$$\begin{aligned} \dot{\phi} &= \frac{C_{dz}(pC_{dz} - rC_{dx}) - C_{dy}(qC_{dx} - pC_{dy})}{C_{dz}^2 + C_{dy}^2} \\ &= p - q\left( \frac{C_{dx} C_{dy}}{C_{dz}^2 + C_{dy}^2} \right) - r\left( \frac{C_{dx} C_{dz}}{C_{dz}^2 + C_{dy}^2} \right) \end{aligned} \tag{4-34}$$

$$\begin{aligned} \dot{\alpha} &= \frac{1}{u^2 + w^2} \left[ u\left( \frac{f_z}{m} + C_{dz} g + qu - pv \right) - w\left( \frac{f_x}{m} + C_{dx} g + rv - qw \right) \right] \\ &= \frac{1}{u^2 + w^2} \left( u\left( \frac{f_z}{m} + C_{dz} g \right) - w\left( \frac{f_x}{m} + C_{dx} g \right) \right) - p\left( \frac{uv}{u^2 + w^2} \right) + q - r\left( \frac{vw}{u^2 + w^2} \right) \end{aligned} \tag{4-35}$$

and

$$\dot{\beta} = \frac{1}{u^2+v^2}\left[u(\frac{f_y}{m} + C_{dy}g + pw - ru) - v(\frac{f_x}{m} + C_{dx}g + rv - qw)\right]$$
$$= \frac{1}{u^2+v^2}\left(u(\frac{f_y}{m} + C_{dy}g) - v(\frac{f_x}{m} + C_{dx}g)\right) + p\left(\frac{uw}{u^2+v^2}\right) + q\left(\frac{vw}{u^2+v^2}\right) - r \qquad (4\text{-}36)$$

These equations can then be combined into a single vector – matrix equation giving

$$\begin{bmatrix}\dot{\phi}\\ \dot{\alpha}\\ \dot{\beta}\end{bmatrix} = \begin{bmatrix} 0 \\ \frac{1}{u^2+w^2}\left(u(\frac{f_z}{m} + C_{dz}g) - w(\frac{f_x}{m} + C_{dx}g)\right) \\ \frac{1}{u^2+v^2}\left(u(\frac{f_y}{m} + C_{dy}g) - v(\frac{f_x}{m} + C_{dx}g)\right)\end{bmatrix} + \begin{bmatrix} 1 & \left(\frac{-C_{dx}C_{dy}}{C_{dz}^2+C_{dy}^2}\right) & \left(\frac{-C_{dx}C_{dz}}{C_{dz}^2+C_{dy}^2}\right) \\ \left(\frac{-uv}{u^2+w^2}\right) & 1 & \left(\frac{-vw}{u^2+w^2}\right) \\ \left(\frac{uw}{u^2+v^2}\right) & \left(\frac{vw}{u^2+v^2}\right) & -1\end{bmatrix}\begin{bmatrix}p\\ q\\ r\end{bmatrix} \qquad (4\text{-}37)$$

It should be noted that this expression is exact in that it required no assumptions about small angle approximations or other linearization, but it does have two potential singularities. The velocity must be nonzero and the definition of roll angle used becomes singular if the vehicle is oriented with the x axis vertical. The first requirement is trivial, and the second can be enforced by redefining the roll angle if vehicle attitude becomes too close to vertical.

Application of the dynamic inversion approach to this model then gives

$$\omega_{cmd} = \begin{bmatrix}p\\ q\\ r\end{bmatrix}_{cmd} = \begin{bmatrix} 1 & \left(\frac{-C_{dx}C_{dy}}{C_{dz}^2+C_{dy}^2}\right) & \left(\frac{-C_{dx}C_{dz}}{C_{dz}^2+C_{dy}^2}\right) \\ \left(\frac{-uv}{u^2+w^2}\right) & 1 & \left(\frac{-vw}{u^2+w^2}\right) \\ \left(\frac{uw}{u^2+v^2}\right) & \left(\frac{vw}{u^2+v^2}\right) & -1\end{bmatrix}^{-1}\left\{\begin{bmatrix}\dot{\phi}\\ \dot{\alpha}\\ \dot{\beta}\end{bmatrix}_{des} - \begin{bmatrix} 0 \\ \frac{1}{u^2+w^2}\left(u(\frac{f_z}{m} + C_{dz}g) - w(\frac{f_x}{m} + C_{dx}g)\right) \\ \frac{1}{u^2+v^2}\left(u(\frac{f_y}{m} + C_{dy}g) - v(\frac{f_x}{m} + C_{dx}g)\right)\end{bmatrix}\right\} \qquad (4\text{-}38)$$

The flight control system designed for the flight tests of a similar vehicle attempted to achieve a 2nd order response with a natural frequency that varied with dynamic pressure. The variation of natural frequency with dynamic pressure was necessary in order to avoid saturation of the control surfaces, which results from attempting to execute rapid maneuvers when the dynamic pressure is low. Given that this vehicle is aerodynamically unstable at higher angles of attack, it is undesirable to saturate the control surfaces for any significant length of time.

The controller required to give the 2nd order desired response can be found from (3-18) as

$$\begin{bmatrix}\dot{\phi}\\ \dot{\alpha}\\ \dot{\beta}\end{bmatrix}_{des} = \begin{bmatrix}w_\phi\\ w_\alpha\\ w_\beta\end{bmatrix} \qquad (4\text{-}39)$$

and

$$\begin{bmatrix} \dot{w}_\phi \\ \dot{w}_\alpha \\ \dot{w}_\beta \end{bmatrix} = \begin{bmatrix} -2\xi\omega_n w_\phi \\ -2\xi\omega_n w_\alpha \\ -2\xi\omega_n w_\beta \end{bmatrix} + \begin{bmatrix} \omega_n^2(\phi_{cmd} - \phi) \\ \omega_n^2(\alpha_{cmd} - \alpha) \\ \omega_n^2(\beta_{cmd} - \beta) \end{bmatrix}. \tag{4-40}$$

In this case the parameters defining the desired 2nd order response are assumed to be the same for the three control axes. Different parameters could easily be used for each axis if desired or different desired responses could be implemented as well. It might well be desirable to use different desired dynamics in the roll axis and the two lateral axes; however, this has not been explored.

## 4.3 Guidance

The inputs to the long period controller as seen in (4-40) are roll angle, angle of attack and angle of sideslip commands. These commands would typically come from guidance algorithms or, perhaps, homing guidance sensors. In order to test the dynamic inversion controller developed here, a simple guidance algorithm that brings the vehicle to level flight at a commanded altitude is implemented. The guidance algorithm is chosen to give a 2nd order dynamic response by taking the commanded acceleration in the vertical direction to be

$$a_d = -\omega_g^2(h_{cmd} - h) - 2\xi_g\omega_g v_d . \tag{4-41}$$

The lateral acceleration commands in body coordinates are then

$$\begin{aligned} a_y &= C_{dy}a_d \\ a_z &= C_{dz}a_d \end{aligned} \tag{4-42}$$

The angle of attack and angle of sideslip commands are found using the lift coefficients as

$$\begin{aligned} \alpha_{cmd} &= \frac{a_z m}{Z_\alpha \bar{q} S_{ref}} \\ \beta_{cmd} &= \frac{a_y m}{Y_\beta \bar{q} S_{ref}} \end{aligned} \tag{4-43}$$

The x acceleration command is ignored. The maximum commanded angles of attack and sideslip are limited to preset values in order to keep the vehicle in a flight envelope in which it can be controlled.

# 5 Implementation

A block diagram of the partitioned dynamic inversion control system is shown in Figure 5-1. The vehicle used in this study has four control surfaces as shown in Figure 1-1. It can be seen that the structure of the control system used is indeed very similar to configuration of more classical approaches. There is a significant difference in that the dynamic inversion blocks are intentionally nonlinear.

The control surface assignment block is used to allocate the control to the three control axes, which results in a 3x3 control matrix and facilitates the application of the dynamic inversion approach.

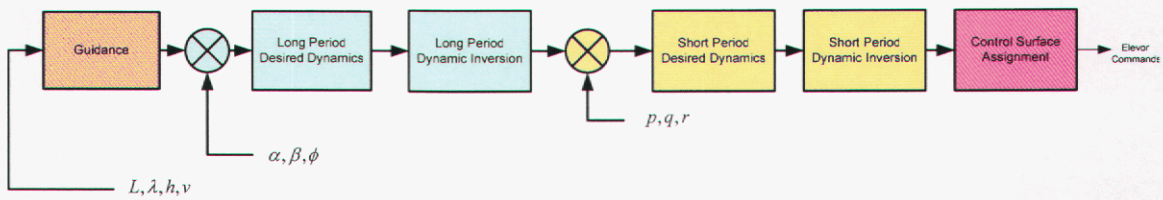


**Figure 5-1. Block diagram of the dynamic inversion control system.**

In this study the roll axis is controlled by differential deflection of all four elevons. The vehicle control input is then taken as

$$\mathbf{u}_{aero} = \begin{bmatrix} \delta_x \\ \delta_y \\ \delta_z \end{bmatrix} = \begin{bmatrix} \delta_R - \delta_L + \delta_B - \delta_T \\ \frac{1}{2}(\delta_R + \delta_L) \\ \frac{1}{2}(\delta_B + \delta_T) \end{bmatrix} \tag{5-1}$$

where $\delta_R, \delta_L, \delta_T$ and $\delta_B$ are the right, left, top and bottom elevon commands, respectively.

We will also assume that the roll (x axis) control is applied equally to the right / left and top / bottom elevon pairs which requires that

$$\delta_R - \delta_L = \delta_B - \delta_T . \tag{5-2}$$

The various aerodynamic parameters are extracted from a trim aero dynamic model stored in tabular form as functions of total angle of attack and aerodynamic roll angle. The aerodynamic model includes reference (i.e. trim) elevon positions, reference body forces and derivatives of both body forces and moments with respect to angle of attack, angle of sideslip and elevon deflections. The total angle of attack and aerodynamic roll angle are computed from measured body velocities derived from the strapdown inertial navigation system. (The effects of wind may be neglected at hypersonic speeds.) The various table entries are interpolated using a two dimensional linear interpolation routine driven by the measured parameters.

In the aerodynamic model the elevon positions are represented as an angle of attack deflection, an angle of sideslip deflection and differential deflections of the angle of attack pair and angle of sideslip pairs.

$$\begin{bmatrix} daatk \\ dasds \\ ddatk \\ ddsds \end{bmatrix} = \begin{bmatrix} \frac{1}{2}(\delta_R + \delta_L) \\ \frac{1}{2}(\delta_T + \delta_B) \\ \delta_R - \delta_L \\ \delta_B - \delta_T \end{bmatrix} . \tag{5-3}$$

The reference parameters utilized in the tabular aerodynamic model are shown in Table 5-1. Table 5-2 shows the various derivatives utilized from the model.

The trim elevon deflections in (4-12) are extracted from the aerodynamic model as

$$\begin{bmatrix} \delta_R - \delta_L \\ \delta_B - \delta_T \\ \frac{1}{2}(\delta_R + \delta_L) \\ \frac{1}{2}(\delta_B + \delta_T) \end{bmatrix}_0 = \begin{bmatrix} ddatk\_ref \\ ddsds\_ref \\ daatk\_ref \\ dasds\_ref \end{bmatrix}. \tag{5-4}$$

The individual trim elevon deflections are then

$$\begin{bmatrix} \delta_R \\ \delta_T \\ \delta_L \\ \delta_B \end{bmatrix}_0 = \begin{bmatrix} daatk\_ref + \frac{1}{2} ddatk\_ref \\ dasds\_ref - \frac{1}{2} ddsds\_ref \\ daatk\_ref - \frac{1}{2} ddatk\_ref \\ dasds\_ref + \frac{1}{2} ddsds\_ref \end{bmatrix}. \tag{5-5}$$

| Parameter | Description |
|---|---|
| aoatk_ref | Angle of attack reference value |
| aosds_ref | Angle of sideslip reference value |
| daatk_ref | Average pitch flap reference value |
| dasds_ref | Average yaw elevon reference value |
| ddatk_ref | Differential pitch elevon reference value |
| ddsds_ref | Differential yaw elevon reference value |
| cfbx_ref | x-axis reference force coefficient |
| cfby_ref | y-axis reference force coefficient |
| cfbz_ref | z-axis reference force coefficient |

**Table 5-1. Reference parameters used in tabular aerodynamic model.**

| Parameters | | | Description |
|---|---|---|---|
| cfbx_aoatk | cfby_aoatk | cfbz_aoatk | Derivatives of force coefficients w.r.t. angle of attack |
| cfbx_aosds | cfby_aosds | cfbz_aosds | Derivatives of force coefficients w.r.t. angle of sideslip |
| cfbx_daatk | cfby_daatk | cfbz_daatk | Derivatives of force coefficients w.r.t. average pitch elevon deflection |
| cfbx_dasds | cfby_dasds | cfbz_dasds | Derivatives of force coefficients w.r.t. average yaw elevon deflection |
| cfbx_ddatk | cfby_ddatk | cfbz_ddatk | Derivatives of force coefficients w.r.t. differential pitch elevon deflection |
| cfbx_ddsds | cfby_ddsds | cfbz_ddsds | Derivatives of force coefficients w.r.t. differential yaw elevon deflection |
| cmbx_daatk | cmby_daatk | cmbz_daatk | Derivatives of moment coefficients w.r.t. average pitch elevon deflection |
| cmbx_dasds | cmby_dasds | cmbz_dasds | Derivatives of moment coefficients w.r.t. average yaw elevon deflection |
| cmbx_ddatk | cmby_ddatk | cmbz_ddatk | Derivatives of moment coefficients w.r.t. differential pitch elevon deflection |
| cmbx_ddsds | cmby_ddsds | cmbz_ddsds | Derivatives of moment coefficients w.r.t. differential yaw elevon deflection |

**Table 5-2. Derivative parameters used in the tabular aerodynamic model.**

The control deflections are found from (5-1) and (5-2) as

$$\begin{bmatrix} \delta_R \\ \delta_T \\ \delta_L \\ \delta_B \end{bmatrix}_C = \begin{bmatrix} \delta_y + \frac{1}{4}\delta_x \\ \delta_z - \frac{1}{4}\delta_x \\ \delta_y - \frac{1}{4}\delta_x \\ \delta_z + \frac{1}{4}\delta_x \end{bmatrix}. \tag{5-6}$$

The control gain matrix in (4-12) is extracted from the aerodynamic model as

$$\mathbf{g}(\alpha_T, \phi_a) = \begin{bmatrix} cmbx\_ddatk + cmbx\_ddsds & cmbx\_daatk & cmbx\_dasds \\ cmby\_ddatk + cmby\_ddsds & cmby\_daatk & cmby\_dasds \\ cmbz\_ddatk + cmbz\_ddsds & cmbz\_daatk & cmbz\_dasds \end{bmatrix} \bar{q} S_{ref} L_{ref} \tag{5-7}$$

where $\bar{q}$ is the dynamic pressure, $S_{ref}$ is the reference area and $L_{ref}$ is the reference length for the vehicle.

# 6 Limitations

In the application of Dynamic Inversion to the control of the reentry vehicle considered here, the theory has been applied to rigid body dynamics of the vehicle and the aerodynamic forces and moments acting on it. The dynamics of the elevon actuators have been ignored, and the theory applied as if the control inputs were applied directly to the control surfaces and the response instantaneous. This is clearly not the case in any practical control system design. The actuator dynamics could be included in model used in the controller formulation, but the advantage of doing so is not clear. The elevon control system, including the actuators, represents a distinct subsystem. The design of the servo actuators is generally executed to achieve some set of performance requirements for the subsystem. To include the actuator states in the Dynamic Inversion controller will have the effect of altering the servo design of the actuators. The elevon control system will have hard limits on the allowable control surface deflection and limits on the slewing rates because of limited drive capability of the actuator motors. When the actuators reach saturation, the control matrices will become singular, thus violating a requirement for the application of the theory.

In theory, Dynamic Inversion transforms a given system into a system of $1^{st}$ order uncoupled differential equations. With appropriate implementation of the control law, any desired response can be achieved. There are clearly limitations to this. Implementation of poorly chosen desired dynamics will likely result in saturation of the control surfaces or operation of the actuators in torque or slew rate limits. In this implementation, the actuator dynamics, which were not included in the control law formulation, can ultimately make the control system unstable -and surely will if the desired dynamics or actuator characteristics are poorly chosen. The Dynamic Inversion formulation developed here proves a concise, systematic method for design of the flight control system. It should not, however, be considered a substitute for analysis of classical control system margins and prudent design practices.

In the formulation presented here, only the rigid body dynamics were considered in implementing the control laws. In the flight test program of a similar vehicle, the elastic body modes of the reentry vehicle and the interaction of the control system with those modes proved to be a formidable challenge. It is likely that some filtering and loop shaping will have to be included in order to provide adequate stability margin against structural mode interactions and instabilities caused by the body bending modes.

The evaluation of the control system performance including the effects of actuator dynamics, can be evaluated using simulation. Evaluation of the potential effects of elastic body modes is beyond the scope of this work.

# 7 Simulation Results

A nonlinear six degree of freedom simulation was developed in order to evaluate the performance of the dynamic inversion controller and to compare it qualitatively to the performance of the system designed for the vehicle flight tested. The simulation of the vehicle dynamics and the control system was implemented using Matlab and Simulink. The Simulink block diagram of the simulation is shown in Figure 7-1. The rigid body dynamics section included a high fidelity, nonlinear model of the attitude dynamics and kinematics.

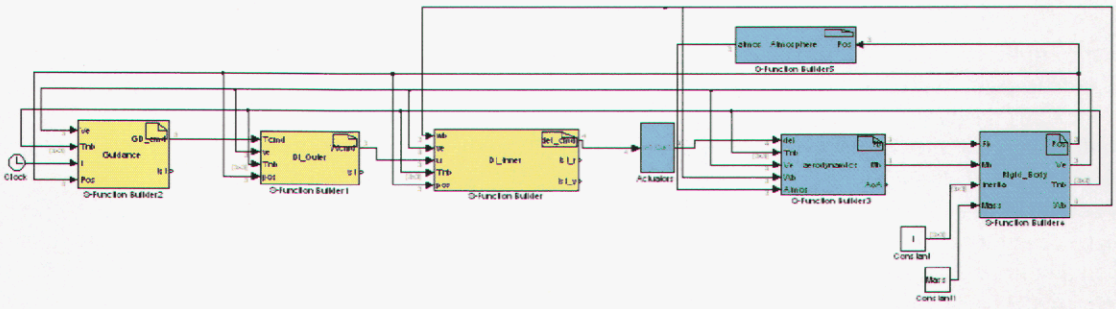

**Figure 7-1. Block diagram of the Simulink non-linear six degree of freedom simulation.**

The aerodynamic model used in the simulation can be input independently of the model used in the simulation of the control system blocks. Additionally, each parameter of the aerodynamic model can be perturbed by a multiplicative factor. The atmospheric model is based on the U.S. Standard Atmosphere. The actuator block contains four 2nd order nonlinear actuator models that include a deflection limit and a slew rate limit. The characteristics of the actuators are shown in Table 7-1.

| Parameter | Value |
|---|---|
| Natural Frequency | 20.0 Hz |
| Damping Constant | 0.707 |
| Deflection Limit | 20.0 Degrees |
| Slew Rate Limit | 200.0 Degrees/Second |

**Table 7-1. Table showing parameters of the simulated elevon actuators.**

The simulation starts with the vehicle at 300,000 feet at a speed of 12,500 feet per second and a vertical flight path angle of -15°. The initial attitude of the vehicle is set so that the roll angle, angle of attack and angle of sideslip are all zero. When the altitude reaches 250,000 feet, the inner control loop is activated. When the vehicle reaches 125,000 feet, the outer control loop and the guidance algorithms are activated and the vehicle commanded to control the altitude to a value of 80,000 feet. During this phase, the magnitude of the commanded angle of attack is limited to ten degrees. The roll angle command is set to a preset value during the pull-out phase, and the angle of sideslip is commanded to zero during this phase. After the vehicle is in level flight a 90° roll command is executed followed by a -45° roll command. The vehicle is then commanded to execute a +10° sideslip command followed by a -15° command.

In the nominal simulation, the natural frequency of the long period desired response is set to 3.0 radians per second, and the damping constant is set to one. The natural frequency is varied with dynamic pressure in the nominal simulation using

$$\omega_n = \begin{cases} 3 & ; \quad \bar{q} < 1000 \\ 3\sqrt{\dfrac{\bar{q}}{1000}} & ; \quad 1000 \le \bar{q} \le 10000 \\ 3\sqrt{10} & ; \quad \bar{q} > 10000 \end{cases} \tag{7-1}$$

The results of the nominal simulation are shown in Figure 7-2 through Figure 7-11. Figure 7-12 shows a subset of the same parameters for a simulation where the aerodynamics of the vehicle are for a 68% center of gravity. Figure 7-13 shows the same parameters for a simulation where the aerodynamics are for a 70% center of gravity. In both cases the nominal (69% center of gravity) aerodynamic model was used in the dynamic inversion control design. It can be seen that the stability characteristics of the vehicle are quite good for both cases. An error in the achieved angle of attack and angle of sideslip can be seen in both cases; however, the vehicle is still able to effect a pull-out at the commanded altitude. Figure 7-14 shows simulation results where the natural frequency in the elevon actuator model is reduced by half to 10.0 Hz.

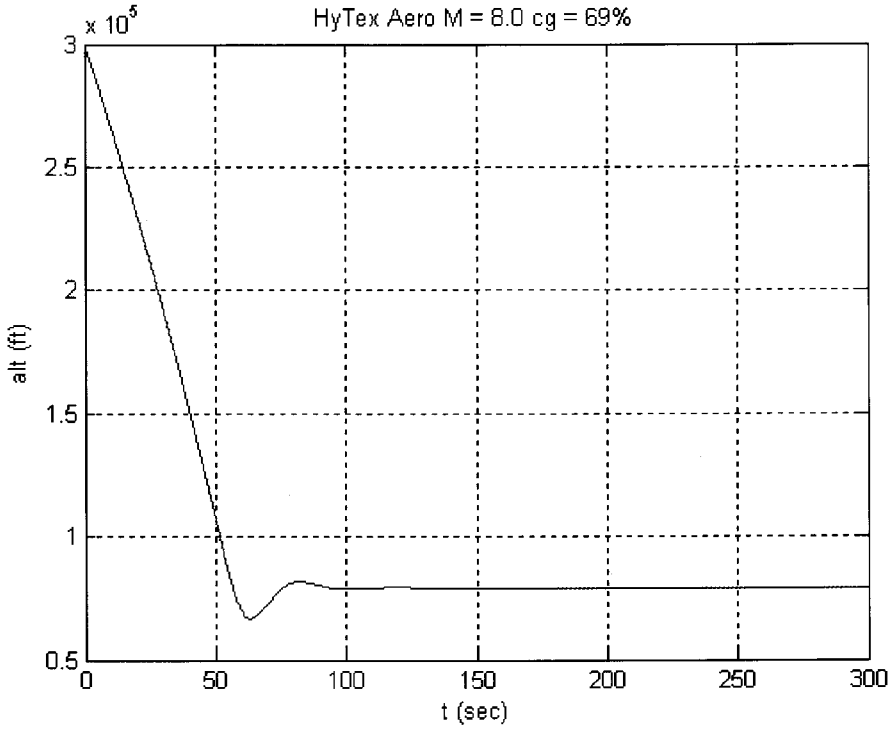


**Figure 7-2. Plot of altitude (in feet) for the nominal simulation.**

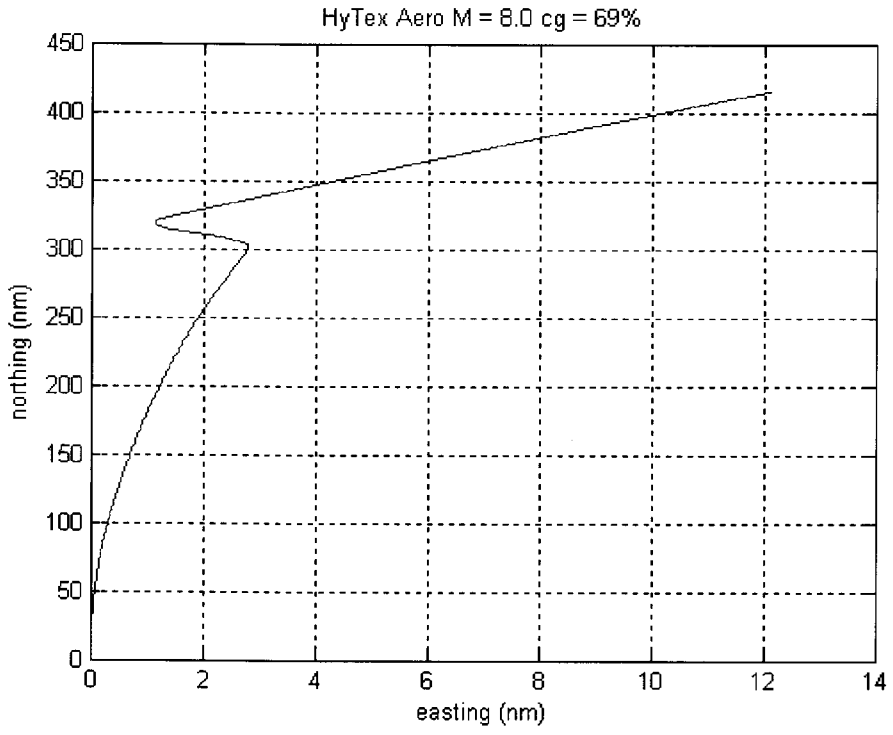


**Figure 7-3. Ground track for nominal simulation.**

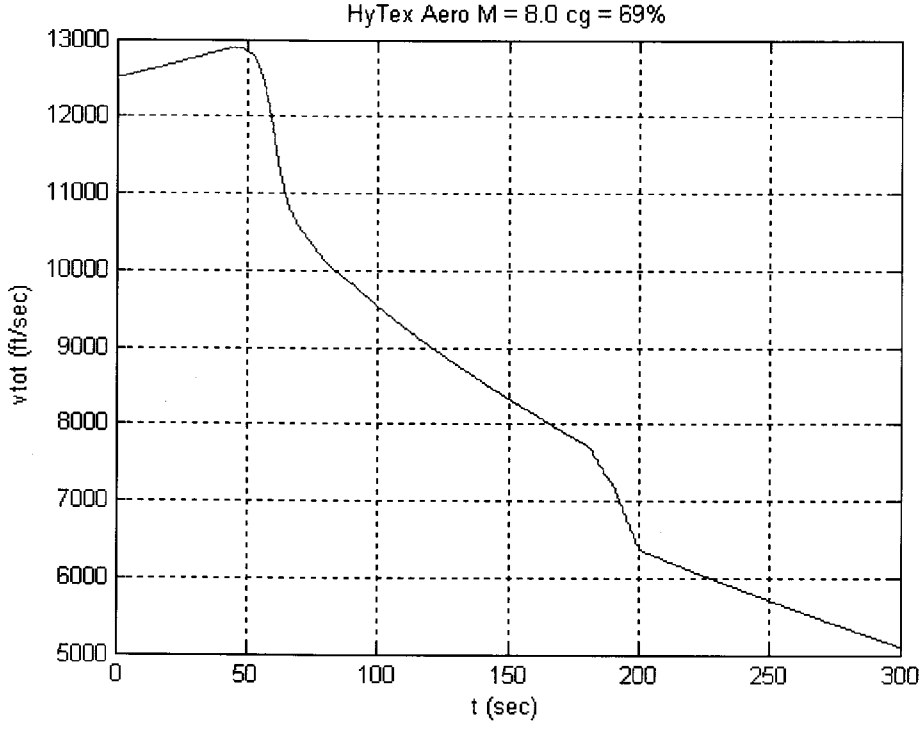


**Figure 7-4. Total velocity in feet per second for the nominal simulation.**

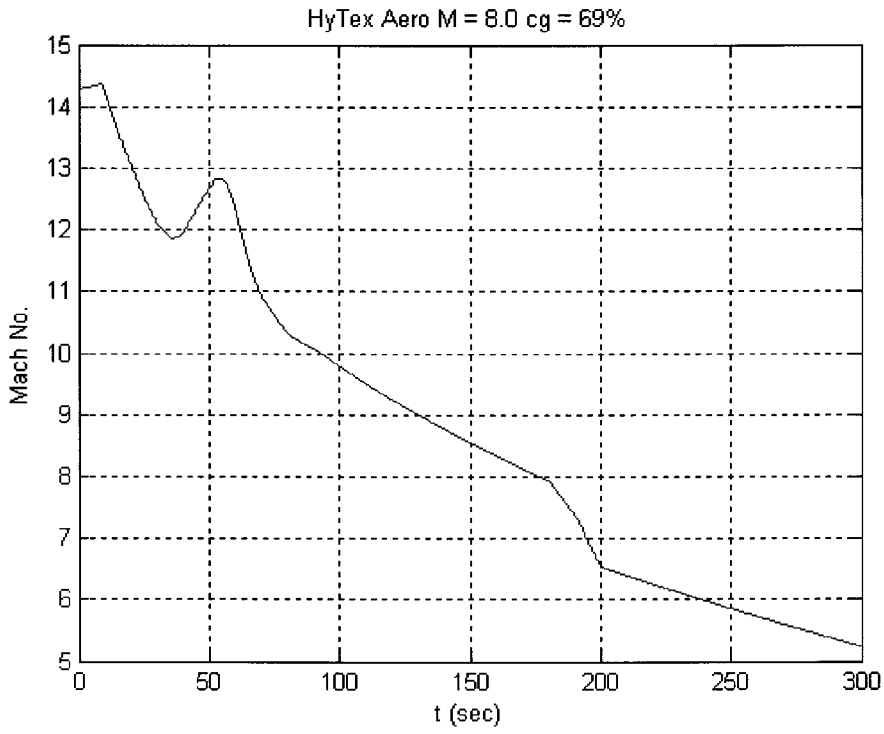


**Figure 7-5. Mach number for the nominal simulation.**

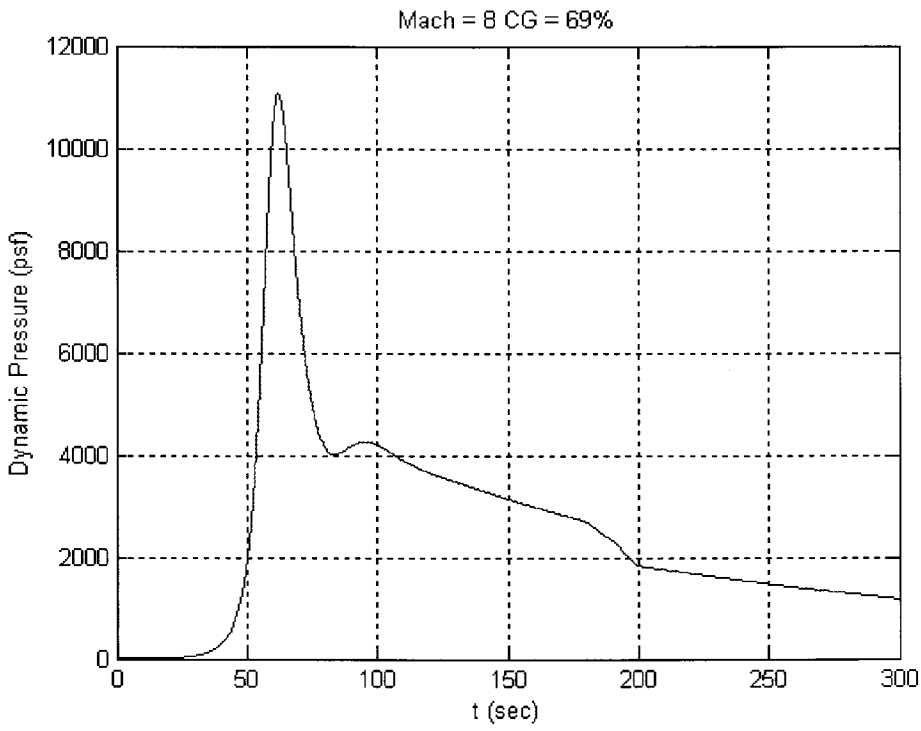


**Figure 7-6. Dynamic pressure in pounds per square foot for the nominal simulation.**

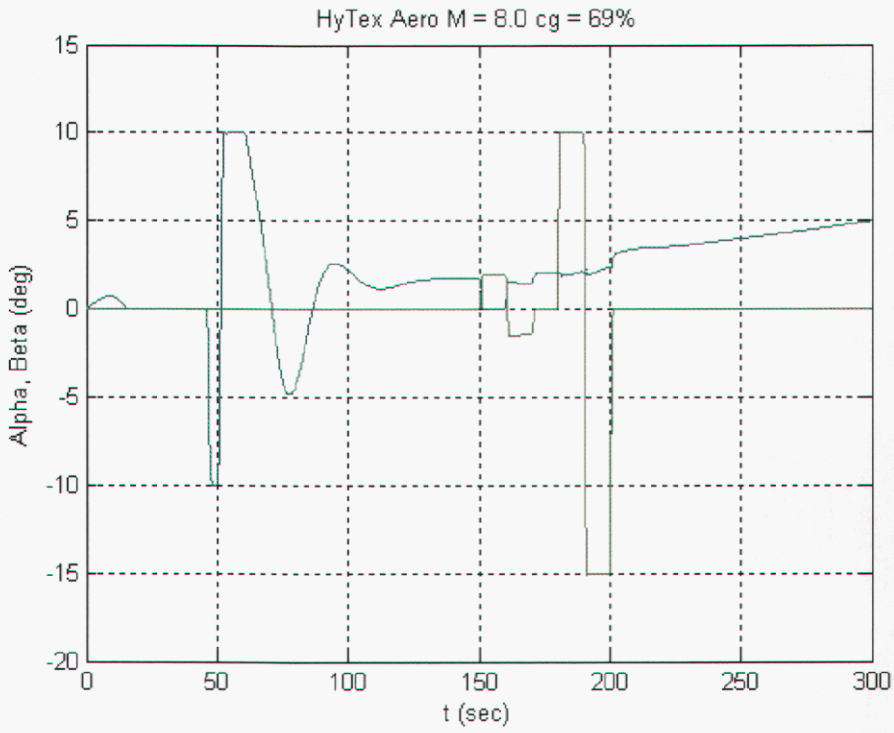


**Figure 7-7. Angle of attack (blue) and angle of side slip (green) in degrees for the nominal simulation.**

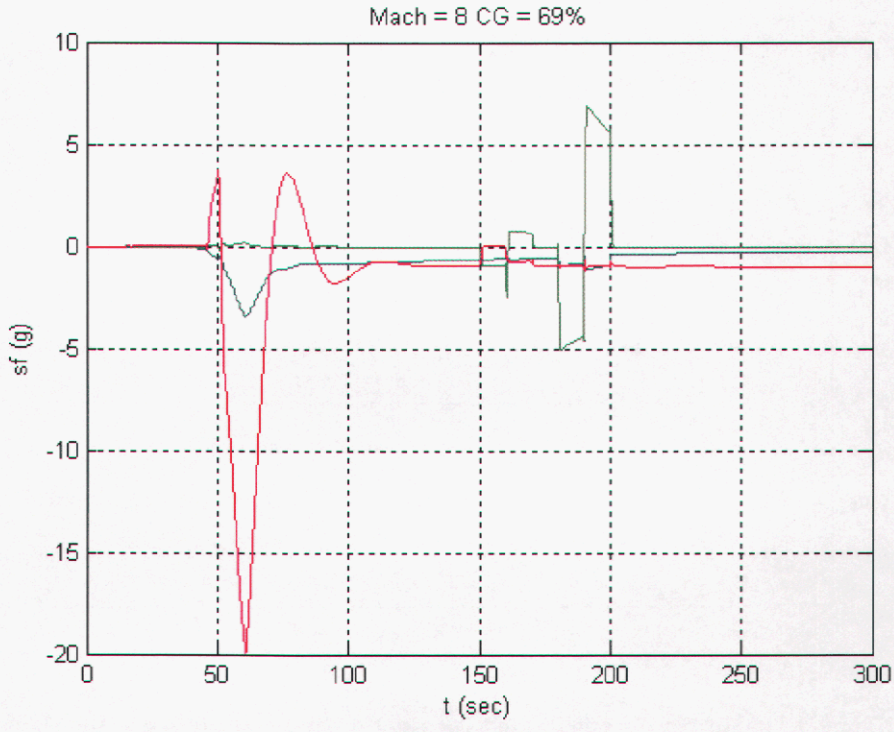


**Figure 7-8. Body specific force (x – blue, y - green, z – red) in G's for the nominal simulation.**

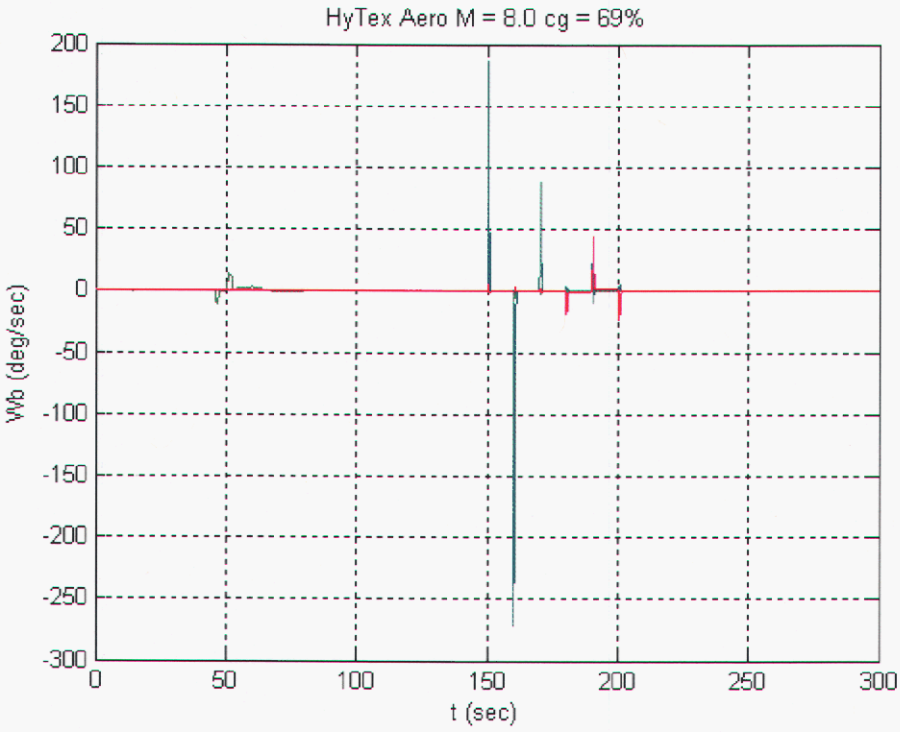


**Figure 7-9. Body angular rates (x – blue, y – green, z – red) in degrees per second for the nominal simulation.**

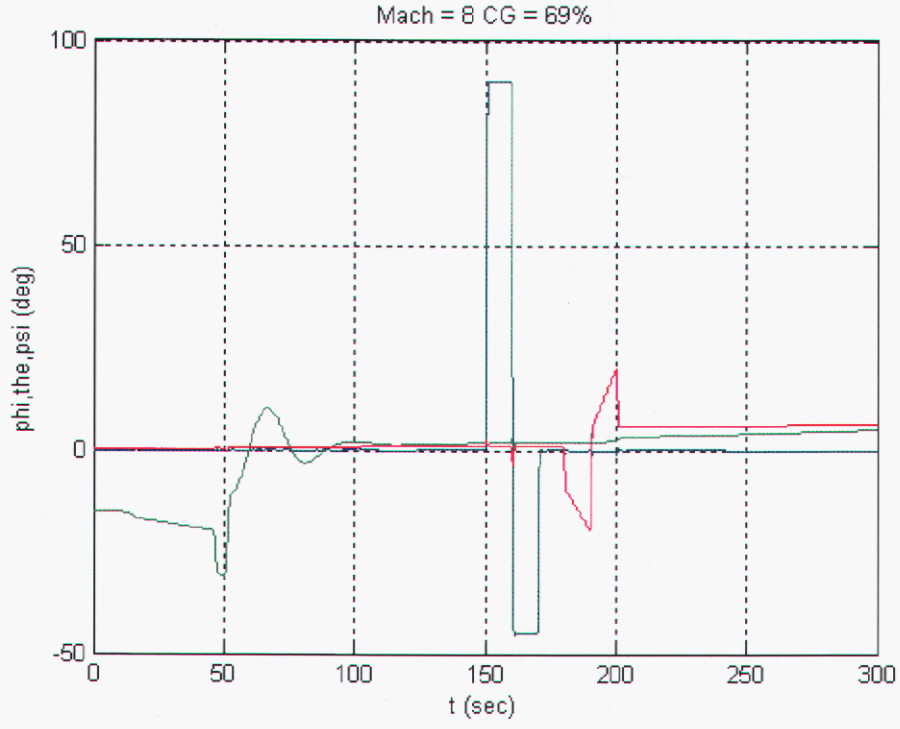


**Figure 7-10. Roll (blue), pitch (green) and yaw (red) angles in degrees for the nominal simulation.**

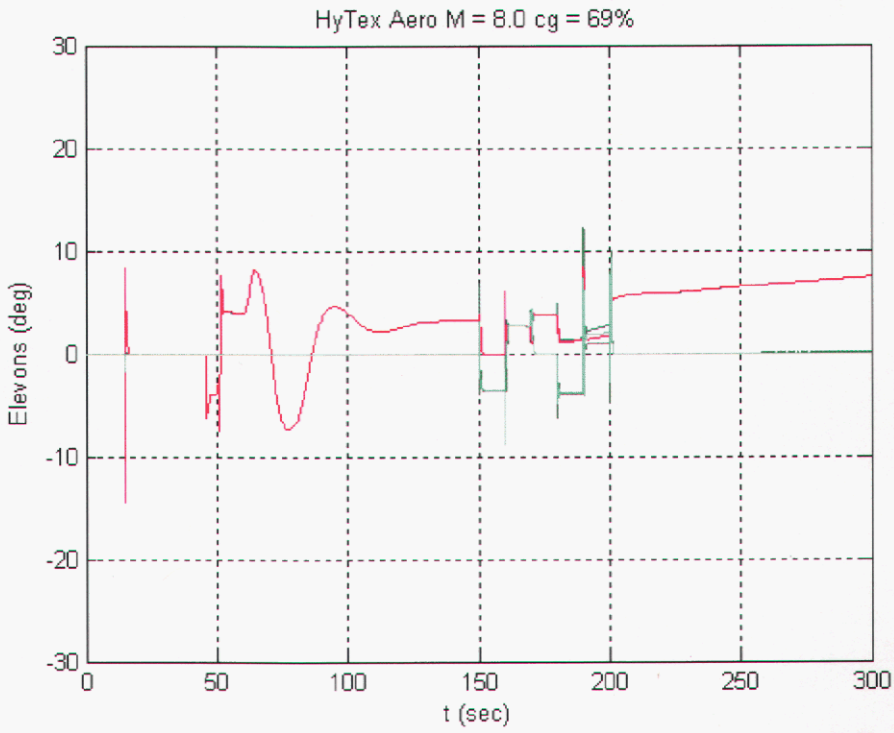


**Figure 7-11. Elevon positions in degrees for the nominal simulation.**

Figure 7-15 shows the results of a simulation where first order desired dynamics were used for the long period desired dynamics. It can be seen that some of the responses appear to overshoot more than the previous case and that the elevon deflections tend to be larger. The larger deflections and the more frequent saturations of the control surfaces are undesirable. Figure 7-16 shows simulation results for a case where the natural frequency of the desired long period second order response was constant rather than varied with dynamic pressure. In this case the nominal response was not significantly degraded, but additional simulations showed that the system was not as robust as the nominal case. Figure 7-17 shows a simulation where the vehicle is commanded to do a slow roll during the pull-up phase of flight. The roll starts when the pull-up is initiated and continues though a complete revolution. In addition to being an interesting demonstration of effectiveness of the control system, it is a maneuver that could be attractive to mitigate the effects of reentry heating.

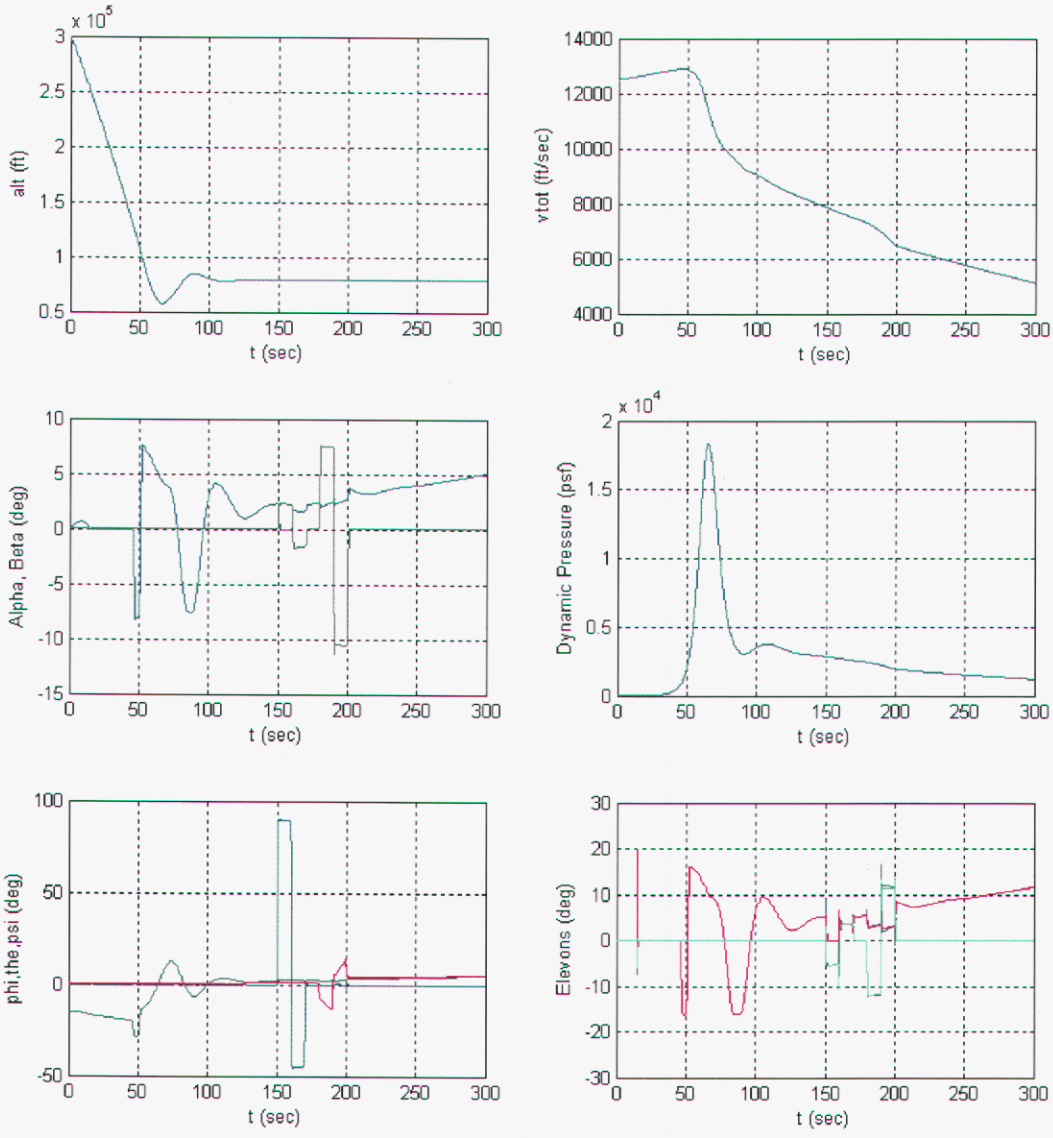


**Figure 7-12. Simulation results for CG = 68%.**

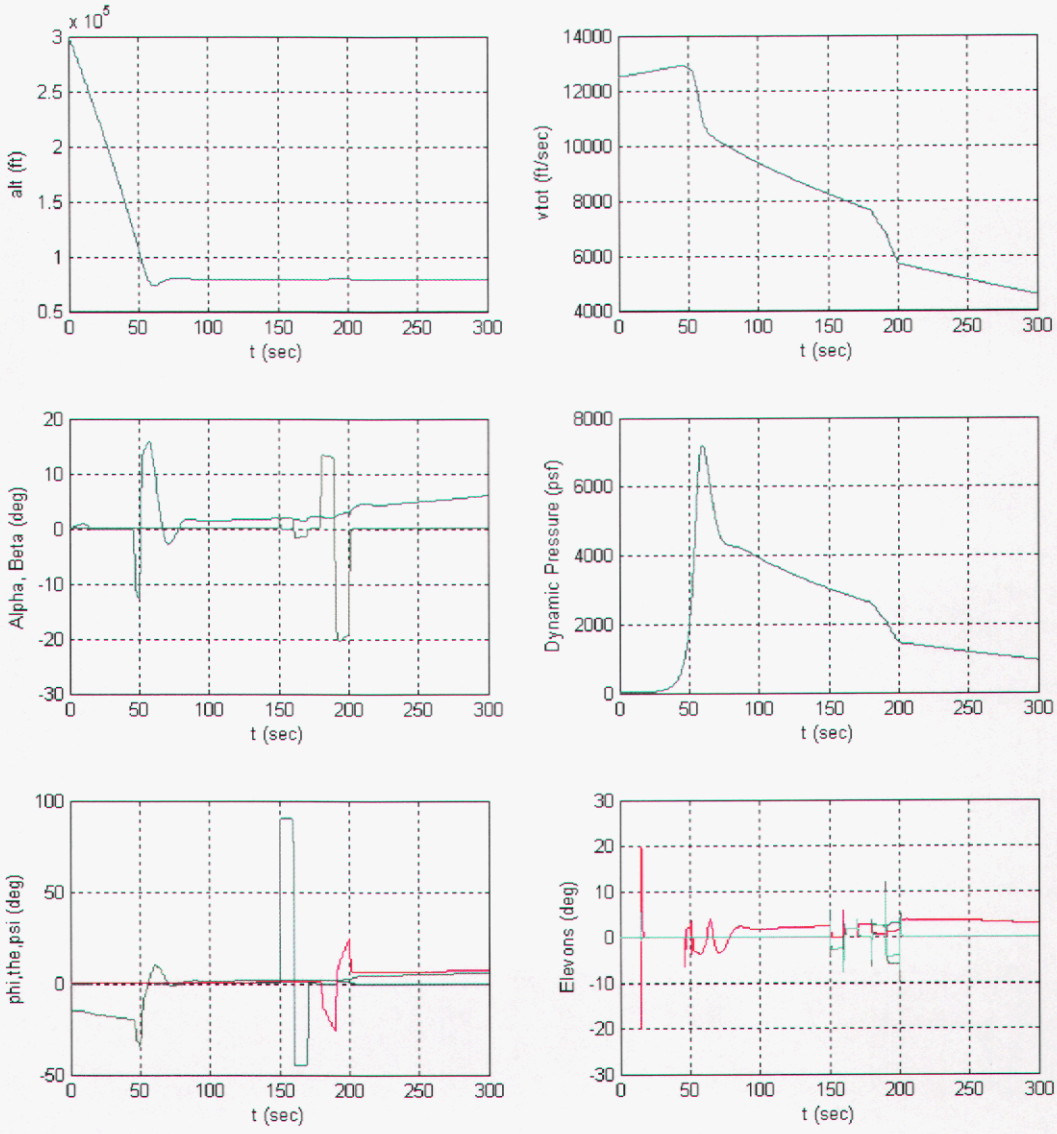


**Figure 7-13. Simulation results for CG = 70%.**

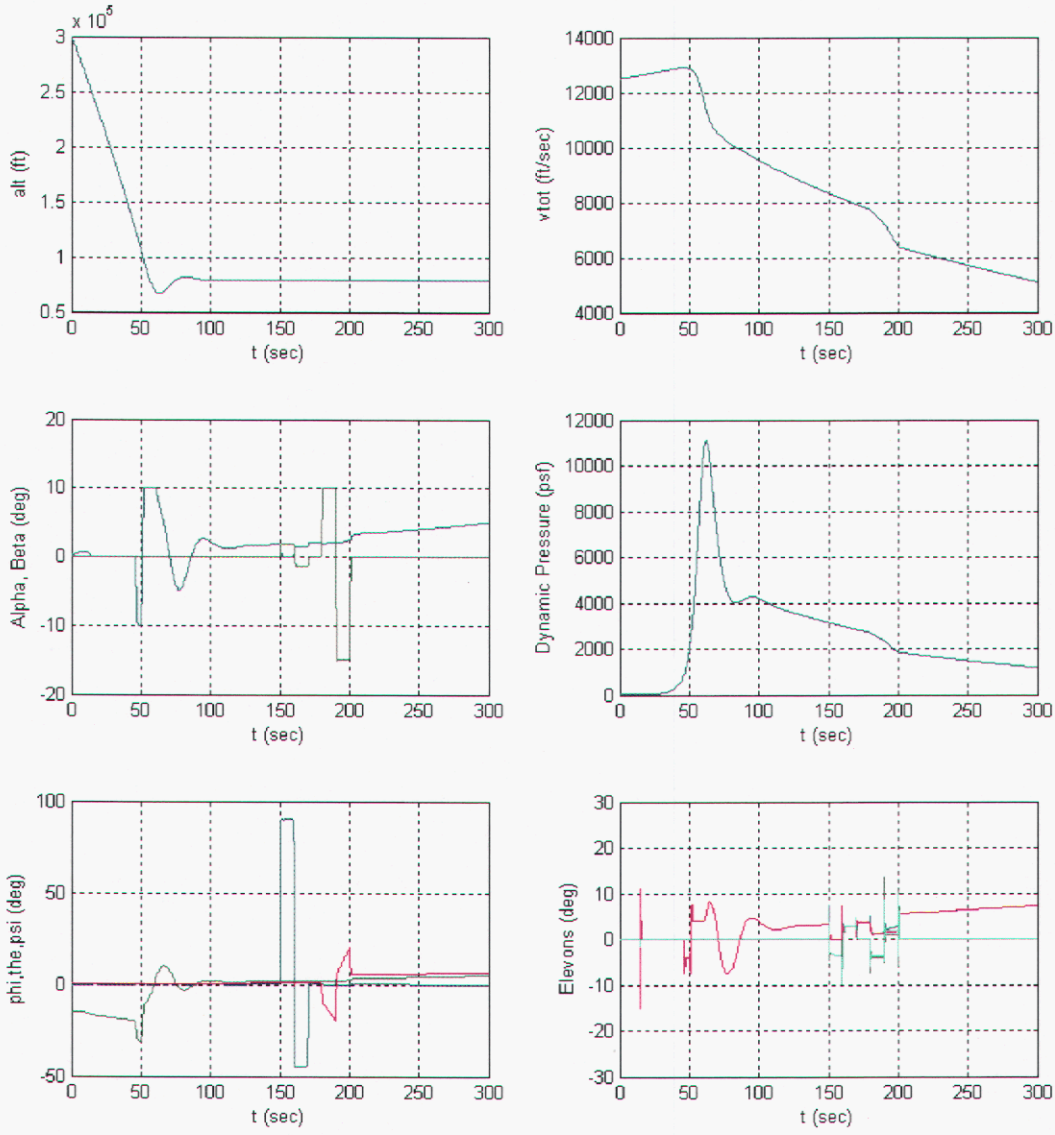


**Figure 7-14. Simulation results with actuator bandwidth reduced to 10 Hz.**

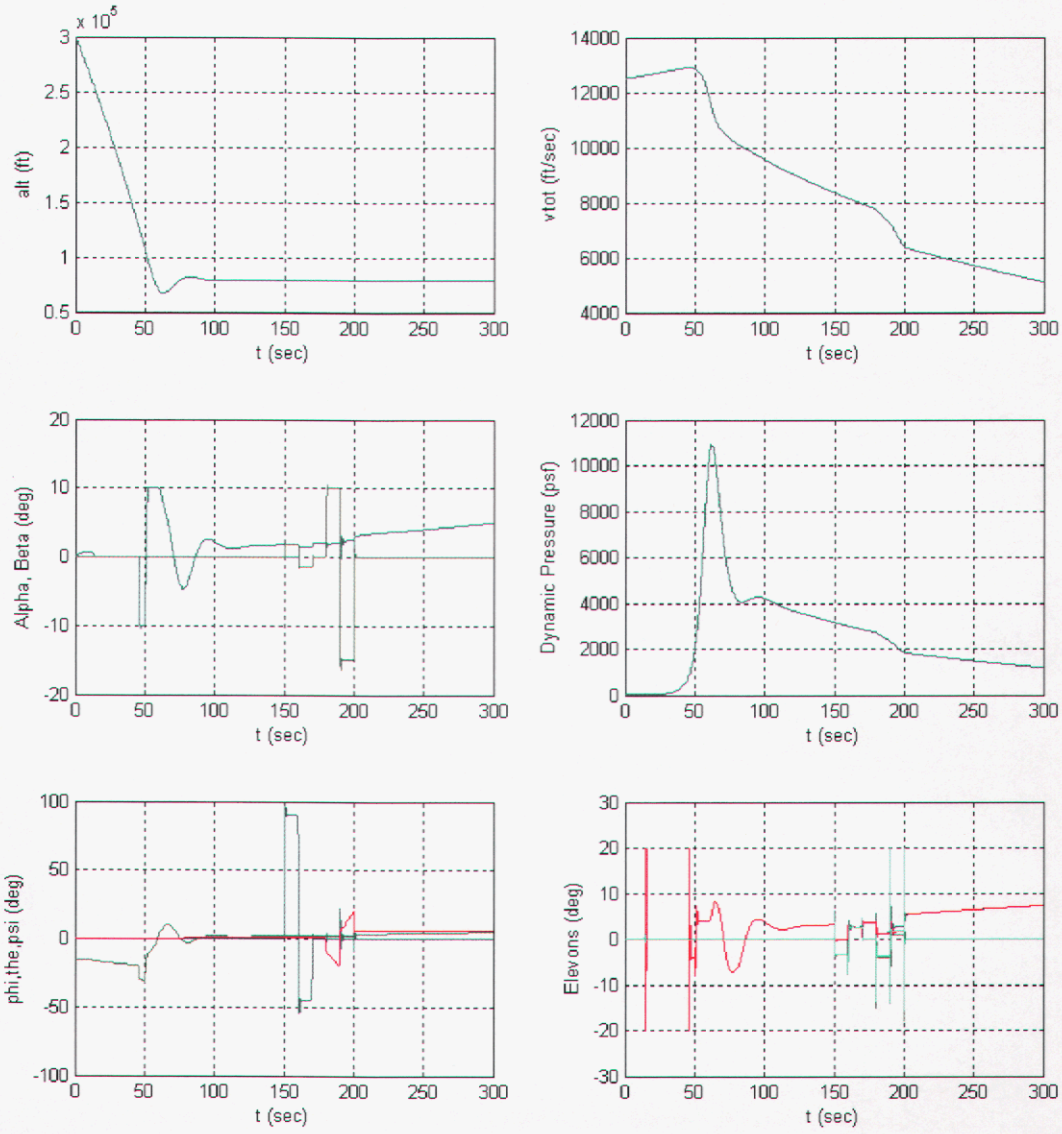


**Figure 7-15. Simulation with 1st order long period desired dynamics.**

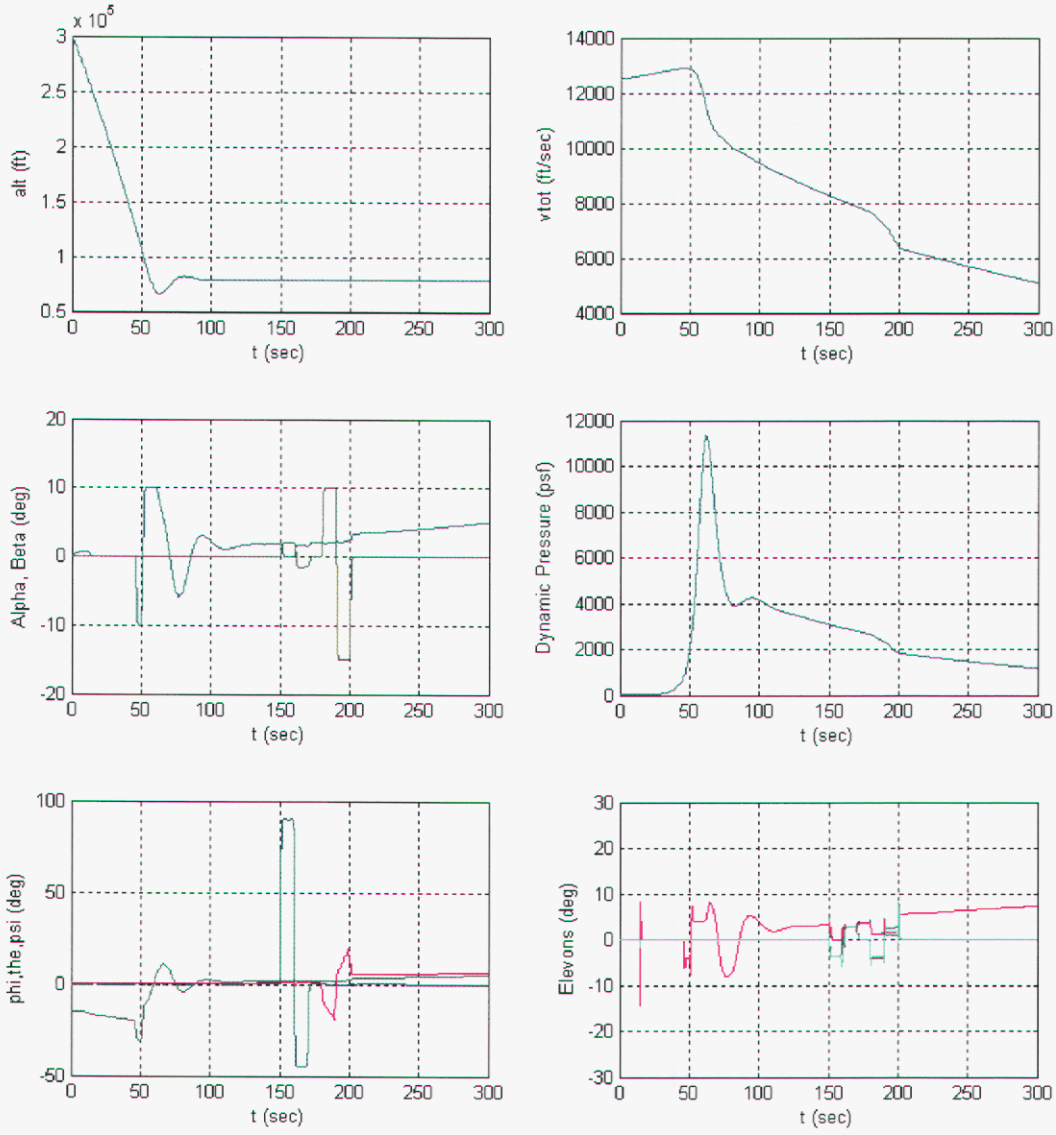


**Figure 7-16. Simulation results with fixed bandwidth 2nd order long period desired dynamics.**

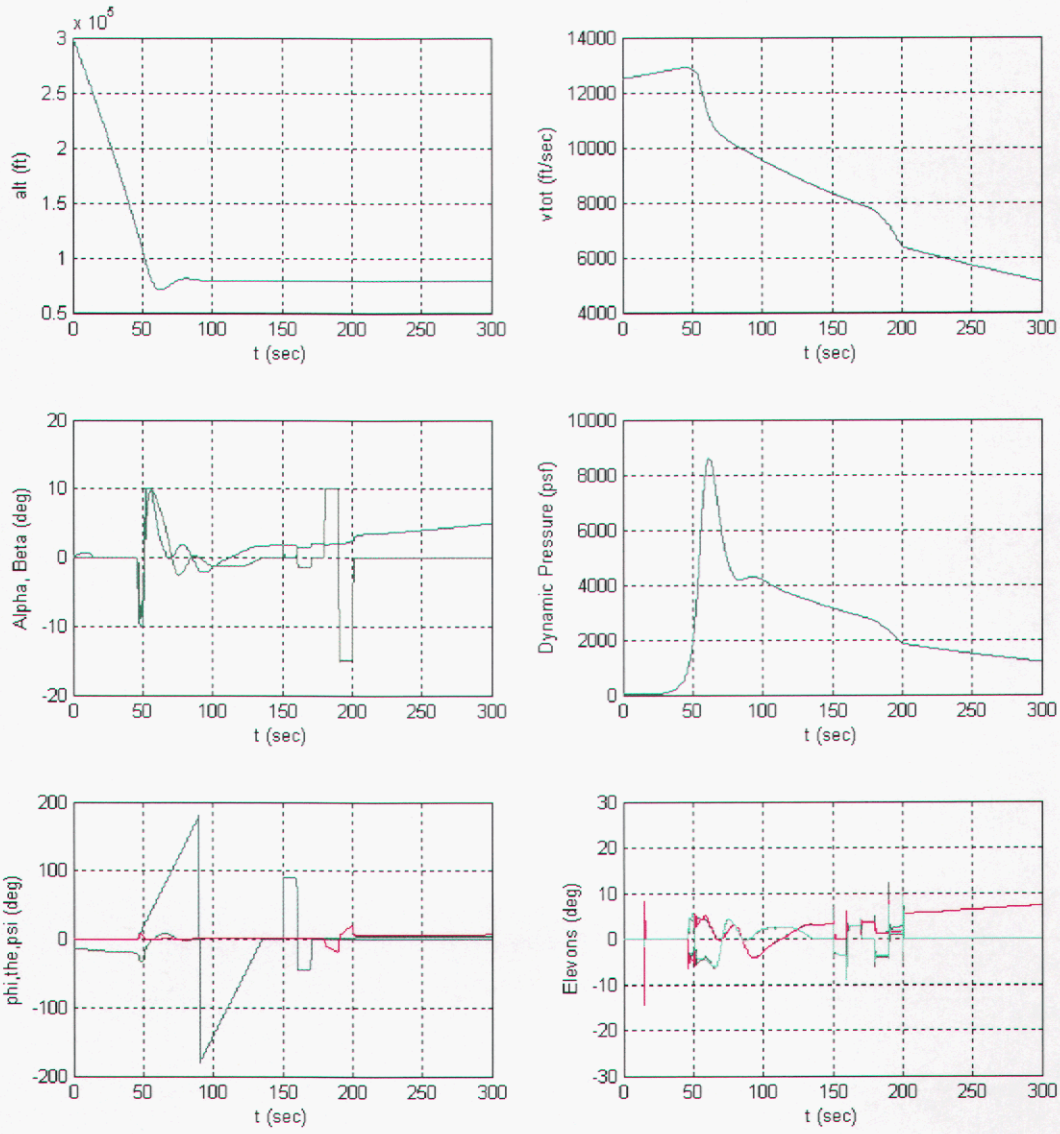


**Figure 7-17. Simulation results where vehicle is commanded to do a 360 degree roll during pull-up.**

# 8 Conclusions

Dynamic Inversion has been successfully applied to the design of flight control algorithms for a high $\beta$ maneuvering reentry vehicle. The aerodynamics of the vehicle used for the purposes of this study are complex and nonlinear at high angles of attack. The vehicle also exhibits induced roll moments and roll-yaw coupling at high angles of attack. In order to perform the required maneuvers for a representative mission, the center of gravity of the vehicle is selected so that it is neutrally stable at zero angle of attack and becomes unstable as the angle of attack increases. Successful designs of flight control algorithms for this vehicle using classical control system design techniques are difficult or impossible for all but experienced control system designers. Dynamic Inversion proved to provide a much more structured design approach and yielded a control design with superior performance that was more robust than designs for similar vehicles executed using classical design approaches.

The basic Dynamic Inversion approach was reformulated to effectively utilize a trim aerodynamic model in the implementation of the flight control algorithms. A systematic approach for implementing a desired dynamic response was developed and applied. A two time scale method suggested by other researches in the area was used in which dynamic inversion was applied to the short period attitude dynamics of the vehicle and the long period dynamics associated with angle of attack and angle of sideslip. A first order response was selected for the short period dynamics, and a second order response with variable natural frequency and damping constant was selected for the long period controller. The resulting structure is similar to the inner loop / outer loop structure used in classical designs but differs in that the control functions used are nonlinear. An exact dynamic model of the roll attitude, angle of attack and angle of sideslip were developed from first principles for use in the long period Dynamic Inversion controller.

A six degree of freedom nonlinear simulation was developed for evaluation of the Dynamic Inversion controllers. The simulation was started at re-entry, and the vehicle was commanded to pull out into level flight and execute several roll and lateral maneuvers. The trajectory used was similar in some respects to the flight test trajectory of a similar vehicle. A simple guidance algorithm was defined to control the simulated vehicle. The dynamic response of the vehicle proved to be excellent. The dynamic response appeared to represent well the chosen $2^{nd}$ order desired dynamic response. The simulation showed no undesirable coupling between the lateral and roll axes of the closed loop control system.

The robustness of the Dynamic Inversion controller was evaluated by using the nominal aerodynamic model of the vehicle for design of the controller, but using off-nominal aerodynamic models for the simulated vehicle. Following the approach used in earlier programs, the primary means of assessing off-nominal aero was to vary the center of gravity used in generating the model used in the simulation. The center of gravity of the nominal vehicle was chosen as 69% of vehicle length. The models used in the simulated aerodynamic models were generated with the center of gravity at 68% and 70%. With the center of gravity at 68%, the vehicle is significantly more stable than the nominal vehicle. The accuracy of the control system in achieving the commanded angle of attack was somewhat degraded, but the control system appeared to be very stable. Likewise, with the 70% center of gravity the vehicle is aerodynamically unstable at all angles of attack. Again, the accuracy of the control system in achieving command angles of attack was degraded, but the control system was stable and the responses were clean and crisp. In both cases the control system was able to fly the required profile, although the minimum altitude during the pull out maneuver and thus the maximum dynamic pressure did vary because of the loss of accuracy in achieving commanded angles of attack. The sensitivity of the design to actuator bandwidth was evaluated by reducing the bandwidth of the simulated actuators by a factor of two to 10.0 Hz. The performance of the Dynamic Inversion controller with the slower actuators was impressive.

The guidance algorithms used in the simulation were modified to command a slow roll through a complete revolution during the pull out maneuver. Such a maneuver would be desirable in order to distribute aerodynamic heating during the high heating rate pull out phase of a flight. The Dynamic Inversion controller executed this maneuver well, with no evidence of roll oscillations or transients.

One disadvantage of the Dynamic Inversion controller observed was the tendency to require large control surface transient deflections. Allowing the control surfaces to saturate on an aerodynamically unstable vehicle is undesirable and potentially catastrophic. The simulation included a limit on deflection and, although the Dynamic Inversion controller did drive the control surfaces to this limit for short periods, the length of time in saturation was short enough to prevent any significant attitude transients. It was found that implementation of 1st order desired dynamics in the outer loop increased the magnitude of control surface deflections. As expected, the commanded control surface deflections increased at lower dynamic pressure, which tended to exacerbate this problem. Using the approach taken in the earlier flight test of a similar vehicle, the natural frequency of the desired 2nd order response was allowed to vary with dynamic pressure in order to minimize control surface deflections during the initial, low dynamic pressure phase of the reentry.

Dynamic Inversion has been shown to be an effective approach for the design of flight control architectures and algorithms for high performance aircraft and low $\beta$ reentry vehicles such as lifting bodies and other vehicles proposed for crew return from orbit. It also appears from this study that the method is very effective and has many advantages for high performance vehicles in reentry trajectories that are representative of long range missile systems. The Dynamic Inversion controller developed here compared very favorably to the design developed for a previous flight test of a vehicle with a similar aerodynamic configuration. The design appeared to be superior in many respects and the approach has the advantage of being more systematic and structured. It should be noted, however, that the Dynamic Inversion design has been proven in a limited study using six degree of freedom simulation. Extensive evaluation of the approach in a comprehensive study in preparation for a flight test might well reveal issues not discovered in this study.

---

## References

[1] Getz, Neil H., "Dynamic Inversion of Nonlinear Maps with Applications to Nonlinear Control and Robotics", Ph.D. dissertation, University of California at Berkeley, 1995.

[2] Ito, D., Georgie, J., Valasek, J. and Ward, D., "Re-Entry Vehicle Flight Controls: Design Guidelines: Dynamic Inversion", Final Technical Report, NAG9-1085, Texas A&M University, May 2001.

## Distribution:

| | | |
|---|---|---|
| 1 | MS 0415 | C. A. Drewien, 9741 |
| 1 | MS 0417 | W. H. Ling, 9743 |
| 1 | MS 0421 | W. C. Hines, 9740 |
| 1 | MS 0825 | B. Hassan, 9115 |
| 1 | MS 1162 | W. H. Rutledge, 15414 |
| 1 | MS 1164 | W. Guyton, 15400 |
| 1 | MS 1174 | E. E. Creel, 15416 |
| 1 | MS 1174 | R. E. Caicedo 15416 |
| 1 | MS 1174 | C. L. Cook, 15416 |
| 1 | MS 1174 | T. M. Criel, 15416 |
| 1 | MS 1174 | R. W. Greene, 15416 |
| 1 | MS 1174 | M. B, Hinga, 15416 |
| 1 | MS 1174 | J. R. Madsen, 15416 |
| 1 | MS 1174 | M. E. Meindl, 15416 |
| 1 | MS 1174 | A. M. Oczon, 15416 |
| 1 | MS 1174 | D. E. Outka, 15416 |
| 1 | MS 1174 | J. R. Phelan, 15416 |
| 1 | MS 1174 | D. D. Stokebrand, 15416 |
| 1 | MS 1174 | R. D. Tucker, 15416 |
| 1 | MS 1174 | R. Wells, 15416 |
| 10 | MS 1174 | A. C. Watts, 15400 |
| 1 | MS 1174 | J. E. White, 15426 |
| 1 | MS 1183 | E. J. Schindwolf, 15420 |
| 1 | MS 1221 | J. L. McDowell, 15000 |
| 1 | MS 1221 | D. L. Keese, 15110 |
| 1 | MS 9018 | Central Technical Files, 8945-1 |
| 2 | MS 0899 | Technical Library, 9616 |